# A comparative study on the *in vivo* behavior of hydroxyapatite and silicon substituted hydroxyapatite granules

N. PATEL*, S. M. BEST, W. BONFIELD
*Department of Materials Science and Metallurgy, University of Cambridge, New Museums Site, Pembroke Street, Cambridge, CB2 3QZ, UK*
*E-mail: np239@cam.ac.uk*

I. R. GIBSON, K. A. HING
*IRC Biomedical Materials, Queen Mary University of London, Mile End Road, London, E1 4NS, UK*

E. DAMIEN, P. A. REVELL
*IRC Biomedical Materials, Royal Free and University College Medical School, Royal Free Campus, Rowland Hill Street, London, NW3 2QG, UK*

Phase pure hydroxyapatite (HA) and a 0.8 wt % silicon substituted hydroxyapatite (SiHA) were prepared by aqueous precipitation methods. Both HA and SiHA were processed into granules 0.5–1.0 mm in diameter and sintered at 1200 °C for 2 h. The sintered granules underwent full structural characterization, prior to implantation into the femoral condyle of New Zealand White rabbits for a period of 23 days. The results show that both the HA and SiHA granules were well accepted by the host tissue, with no presence of any inflammatory cells. New bone formation was observed directly on the surfaces and in the spaces between both HA and SiHA granular implants. The quantitative histomorphometry results indicate that the percentage of bone ingrowth for SiHA (37.5% $\pm$ 5.9) was significantly greater than that for phase pure HA (22.0% $\pm$ 6.5), in addition the percentage of bone/implant coverage was significantly greater for SiHA (59.8% $\pm$ 7.3) compared to HA (47.1% $\pm$ 3.6). These findings indicate that the early *in vivo* bioactivity of hydroxyapatite was significantly improved with the incorporation of silicate ions into the HA structure, making SiHA an attractive alternative to conventional HA materials for use as bone substitute ceramics.


## 1. Introduction

Hydroxyapatite [$Ca_{10}(PO_4)_6(OH)_2$, HA] is well established as a synthetic material for bone replacement due to its chemical similarities to the inorganic component of bone and tooth. However, the mineral phase of bone is not hydroxyapatite, but can be described as a multi-substituted calcium-phosphate apatite. The type and amount of ionic substitution in the apatite phase varies from the wt % level (e.g. 2–8 wt % $CO_3$) to the ppm-ppb level (e.g. $Mg^{2+}$ or $Sr^{2+}$) [1, 2]. The role of many of these ionic species in hard tissues is not fully understood owing to the difficulties encountered in monitoring and quantifying the amounts of ionic content in bone mineral, which vary in composition consequent upon dietary alterations and physiological and pathological causes [3]. However, it is accepted that these different ions play a major role in the biochemistry of bone.

Silicon is believed to be essential in skeletal development, the first indications of a physiological role for silicon were determined by Carlisle [4, 5] who reported that silicon was involved in the early stage of bone calcification. Similarly studies by Schwarz and Milne [6] have shown that silicon deficiency in rats resulted in skull deformations, with the cranial bones appearing more flatter than normal. These early findings suggest a relationship between silicon intake and bone mineralization.

More recent evidence of the role of silicon in bone metabolism can be found in the use of silicon rich materials (bioactive glasses and glass ceramics) that contain high levels of $SiO_2$ (30–50 wt %) [7, 8]. It has been proposed that the bioactivity of these $SiO_2$-rich glass formulations is related to the role of $SiO_2$ or silicon on their surface reactions, and therefore in their *in vivo* and *in vitro* bioactivity [9]. The initial cellular and ionic processes which occur at the surface of bioactive glasses and glass ceramics allow the subsequent crystallization of apatite crystals, cell adhesion and collagen formation.

* Author to whom all correspondence should be addressed.

These reactions in glasses are very rapid and have been reported to occur within minutes of implantation [10], and it is these rapid responses which are thought to make these materials very bioactive.

Since $SiO_2$ or silicon has been shown to enhance the bioactivity of glass-based materials, silicon may also enhance the bioactivity of HA with the incorporation of silicon into the HA structure. HA has the advantage over bioactive glasses and glass ceramics in that it is chemically similar to the inorganic component of bone. Therefore a potential method for improving the bioactivity of hydroxyapatite is the incorporation of silicon into the hydroxyapatite lattice. Many attempts have been made to prepare silicon substituted hydroxyapatites by a variety of synthesis methods, however these have resulted in either silicon containing apatites with undesirable secondary phases [11, 12] or the additional substitution (besides silicon) of ionic groups into the HA lattice [13]. These secondary phases and additional substitutions make it difficult to determine the true role of silicon on the *in vitro* and *in vivo* bioactivity of silicon substituted hydroxyapatite.

A recent study by Gibson *et al*. [14] described the preparation of a silicon substituted hydroxyapatite by an aqueous precipitation method. The resulting silicon substituted hydroxyapatite contained approximately 0.4 wt % silicon, with no indication of any secondary phases such as calcium oxide or tricalcium phosphate. In addition, the authors reported that the *in vitro* bioactivity was substantially enhanced with the incorporation of silicon into the HA lattice [15]. However, *in vitro* tests provide limited information, as they do not simulate the true physiological *in vivo* behavior of the material. To date there have been no reports which compare the *in vivo* bioactivity of SiHA with HA. The aims of this present study were to synthesize and prepare granules of phase pure HA and SiHA, and to assess the effect of silicon substitution on the *in vivo* bioactivity of HA.

## 2. Materials and methods

### 2.1. Sample preparation

Stoichiometric hydroxyapatite was prepared by an aqueous precipitation reaction between calcium hydroxide ($Ca(OH)_2$) and orthophosphoric ($H_3PO_4$) acid solution based on the methods described elsewhere [16–18]. The precipitation reaction was performed at room temperature and the pH was maintained at approximately 10.5 with the addition of ammonia solution. After complete mixing of the reactants, the suspension was aged at room temperature overnight.

A 0.8 wt % silicon substituted HA was synthesized in a similar manner to HA according to the methods described by Gibson *et al*. [14]. The quantities of reactants were calculated on the basis that the number of moles of $H_3PO_4$ in phase pure HA would be equivalent to the number of moles of ($H_3PO_4$ + silicon acetate) in the silicon substituted hydroxyaptite, with the number of moles of $Ca(OH)_2$ kept constant at 0.5. Both sets of filter cakes were processed into green granules (0.5–1 mm) by partial grinding and mechanical sieving. The granules were subsequently sintered to 1200 °C for 2 h in air (Carbolite RHF 1600); the heating rate was 2.5 °C/min and the cooling rate to room temperature was 10 °C/min.

### 2.2. Chemical analysis

The phase composition of both HA and SiHA granules were analyzed by X-ray diffraction (XRD) using a Siemens D5000 diffractometer. Data were collected over the 2θ range 25–40 °C with a step size of 0.02° and a count time of 2.5 s. Identification of the phases was achieved by comparing the diffraction patterns of HA and SiHA with ICDD (JCPDS) standards [19]. The calcium/phosphorus (Ca/P) molar ratios of HA and SiHA were determined by a direct measurement from the X-ray fluorescence (XRF) spectroscopy results. The carbonate contents of the sintered granules were measured by C–H–N analysis (Medac Ltd. UK). Fourier transform infrared (FTIR) spectra were obtained using a Nicolet 800 spectrometer, at a resolution of $4\,cm^{-1}$, averaging 100 scans.

### 2.3. Physical characterization

The bulk density for both sets of sintered granules was determined using a Micromeritics Accupyc 1330 pycnometer. In addition the packing density of the granules was determined using a Micromeritics Geopyc 1360 instrument, by measuring the mass of granules required to fill a container of specified volume. The specific surface area of the granules was determined by the Brunauer–Emmett–Teller (BET) method using a Micromeritics Gemini II 2370 surface area analyzer. Scanning electron microscopy (SEM) of the sintered granules was performed using a field emission JEOL F6300 SEM, which provided information about the morphology and size of the granules.

### 2.4. Implantation procedure

The guidelines for the care and use of laboratory animals (Animals (Scientific Procedures) Act 1986) were observed throughout the implantation procedures. Six month old female New Zealand White rabbits (average weight $\approx 3$ kg) were used for implantation. Prior to surgery granules of sintered HA and SiHA were sterilized at 150 °C for 4 h. The implants were placed bilaterally into the femoral condyle (Fig. 1). Defects approximately 4 mm in diameter and 7 mm in depth were drilled into the patellar groove of the femoral condyle using a saline cooled diamond tip trephine. The sterile granules were press-fitted into the defect prior to suturing. The animals were injected subcutaneously with fluorochrome labels according to the protocol described in Table I, and were sacrificed 23 days after surgery.

### 2.5. Histological evaluation

After sacrifice the implant/bone were fixed in formaldehyde solution and dehydrated using various grades of alcohol, prior to embedding in PMMA resin. Sectioning of the specimen blocks was performed parallel to the longitudinal axis of the tibia using a diamond band saw and an Exakt system for grinding and polishing thin

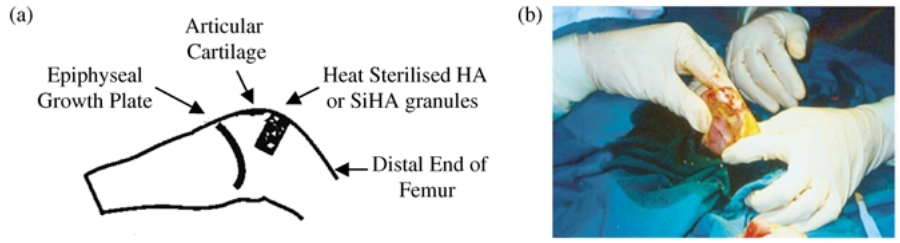


*Figure 1* Position of hydroxyapatite (HA) or silicon substituted hydroxyapatite (SiHA) granular implants, (a) schematic diagram identifying the key points, and (b) photograph of the implant site.

TABLE I Fluorochrome labeling protocol

| Fluorochrome label | Dosage (mg kg$^{-1}$) | Time of label administration (days after surgery) | Appearance under UV light with N.2.1. Leica filter cube | Appearance under UV light with RGB Leica filter cube |
|---|---|---|---|---|
| Tetracycline | 0.5 | 0 | Orange | Yellow |
| Calcein green | 0.5 | 7 | Green | Green |
| Alizarin red | 0.5 | 14 | Red | Red |
| Tetracycline | 0.5 | 21 | Orange | Yellow |

Animals were sacrificed 23 days after surgery.

sections (Exakt Corp., Hamburg, Germany). Sections $\approx 25\,\mu m$ thick were stained with toluidine blue for histological examination and histomorphometry using a Leitz brightfield transmitted optical microscope. Unstained sections also $\approx 25\,\mu m$ thick were examined using a Leica DMRXB UV light optical microscope to detect fluorescent labels.

## 2.6. Histomorphometry

Histomorphometry was performed on micrographs of sections of HA and SiHA taken at magnifications of $\times 25$. A series of images were obtained for each section. These images were stitched together to represent a collage of the whole section. Histomorphometry was performed on each section using linear intercept and point counting methods in order to build up a map of bone ingrowth and bone/implant coverage within each section. The percentage of bone ingrowth was measured for each section using a 42-point Weibel grid [20], a hit for bone ingrowth $(H_{BI})$ was scored when a point fell over an area of bone, as shown in Fig. 2, the percentage of bone ingrowth per Weibel grid $(AG_{\mathrm{BI}})$ was calculated according to Equation 1. The absolute percentage of bone ingrowth for the whole section $(AS_{\mathrm{BI}})$ was determined as a mean of the number $(N_{\mathrm{W}})$ of Weibel grids used per section according to Equation 2.

$$AG_{BI} = \frac{\sum_{i=1}^{i=42} H_{BI_i}}{42} \times 100 \tag{1}$$

$$AG_{BI} = \frac{\sum_{i=1}^{i=N_W} AG_{BI_i}}{N_W} \tag{2}$$

Similarly the coverage of bone ingrowth on the implant surfaces (bone coverage) was measured by placing Merz grids [21] over the section, as shown in Fig. 3. A hit for bone coverage $(H_{\mathrm{BC}})$ was scored when a line intersected a bone/implant interface, similarly a hit for implant/trabecular space $(H_{\mathrm{IS}})$ was scored where a line intersected an implant/trabecular space interface, the percentage of bone coverage per Merz grid $(G_{BC})$ was calculated according to Equation 3. The absolute percentage of bone coverage for the section $(S_{BC})$ was calculated as a mean of the number $(N_M)$ of Merz grids used per section, according to Equation 4.

$$G_{BC} = \frac{\sum_{i=1}^{i=x} H_{BC_i}}{\sum_{j=1}^{i=y} H_{IS_i}} \times 100 \tag{3}$$

$$S_{BC} = \frac{\sum_{i=1}^{i=N_W} G_{BC_i}}{N_M} \tag{4}$$

The fluorochrome labels were used to assess the bone mineral apposition rates (MAR) of HA and SiHA sections. Fluorochrome labels are bound to sites of active bone deposition, shortly after administration. This enables identification of bone deposited at different time points. The mineral apposition rates were calculated by

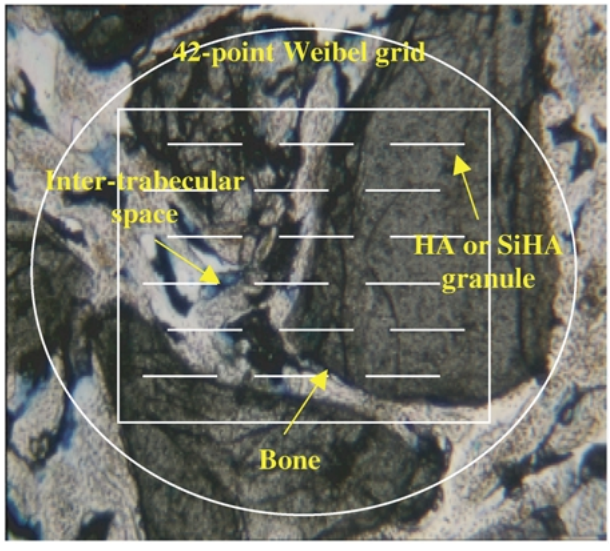


*Figure 2* Measurement of bone ingrowth with a Weibel grid. A hit for bone ingrowth $(H_{BI})$ was scored when a point fell over an area of bone.

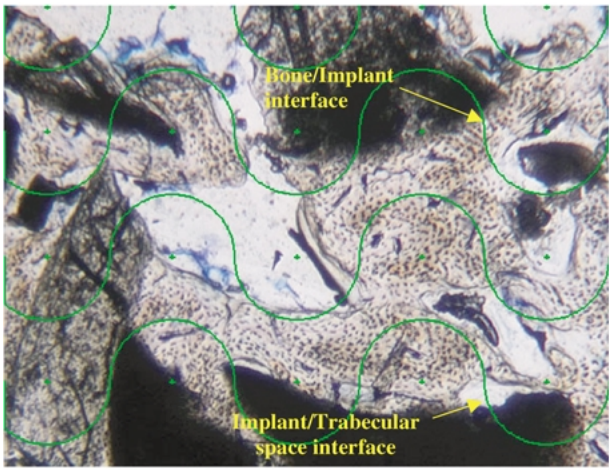


*Figure 3* Measurement of bone coverage with a Merz grid. A hit for bone coverage ($H_{BC}$) was scored when a line intercepted a bone/implant interface. Similarly a hit for implant/trabecular space ($H_{IS}$) was scored when a line intercepted an implant/trabecular space interface.

measuring the mean distance between the three different fluorescent labels, and dividing these distances by the difference in the time-points at which the labels were administrated.

## 3. Results

### 3.1. Chemical analysis

The Ca/P ratio and the principal elements detected by XRF for HA and SiHA are shown in Table II. The Ca/P ratio of HA was found to be equivalent to the theoretical value of phase pure HA (1.67). The Ca/P molar ratio of SiHA (1.74) was much higher than the value for stoichiometric HA. This increase in Ca/P ratio for SiHA is due to the substitution of silicate ions for the phosphate site in HA, in order to accommodate silicate ions, the phosphorus content was decreased. However, if the molar ratio for SiHA is measured as Ca/(P + Si) ratio, then the value of 1.67 is the same as the molar ratio of HA. The amounts of silicon (wt %) as measured by XRF are also shown in Table II. The amount of silicon in the SiHA sample (0.78 wt %) was very close to the expected value (0.8 wt %), the HA granules contained undetectable amounts of silicon as expected. Furthermore, the carbonate contents measured by C–H–N analysis indicate that for both HA and SiHA sintered granules, carbonate content was undetected. The X-ray diffraction patterns of sintered HA and SiHA granules are shown in Fig. 4. The XRD patterns for the two materials appeared to be similar, the incorporation of silicon into the HA lattice did not have a direct affect on the phase composition, with no indication of secondary phases such as calcium oxide (CaO) or tricalcium phosphate (TCP). The diffraction peaks matched the ICDD (JCPDS) standards for HA. Fig. 5 show the FTIR spectra

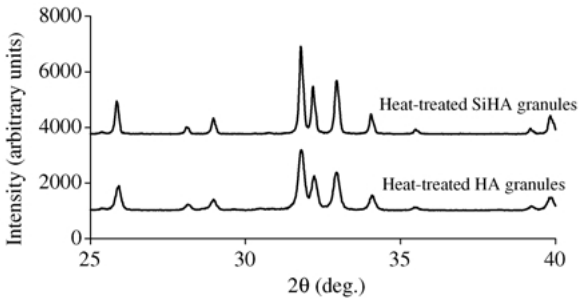


*Figure 4* X-ray diffraction patterns of sintered (1200 °C; 2 h) hydroxyapatite (HA) and silicon substituted hydroxyapatite (SiHA) granules. No secondary phases such as $Ca_3(PO_4)_2$ (TCP) or CaO were detected.

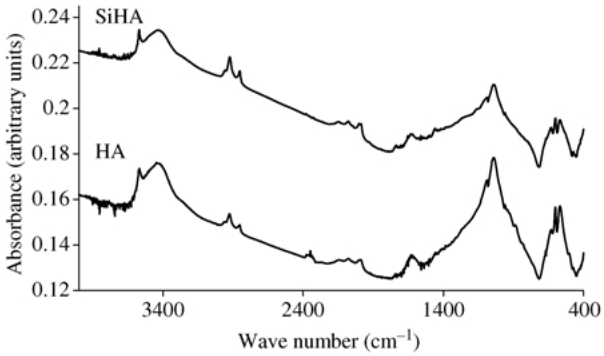


*Figure 5* Fourier transform infrared (FTIR) spectra of sintered (1200 °C; 2 h) hydroxyapatite (HA) and silicon substituted hydroxyapatite (SiHA) granules.

of sintered HA and SiHA and are similar to those observed by Gibson *et al*. [14] with the most notable effect of silicon substitution on the FTIR spectra of hydroxyapatite being the changes in the $PO_4$ bands between 800 and 1100 $cm^{-1}$ and 500–700 $cm^{-1}$.

### 3.2. Physical characterization

The bulk density, packing density and specific surface areas of both sets of granules are listed in Table III. The bulk density for HA and SiHA was found to be 97–99% of the theoretical value (3.156 g $cm^{-3}$). The packing density was similar for both HA and SiHA granules indicating that the same mass of granules for both cases would be required to fill defects of known volume. The specific surface areas of the sintered granules were also similar. Fig. 6 shows SEM images of sintered HA and SiHA granules, both sets of granules were similar in size and morphology.

### 3.3. Histological evaluation

Extensive osseointegration was observed in both HA and SiHA implants with seams of osteoblasts depositing bone

TABLE II Chemical analysis of sintered HA and SiHA granules using X-ray fluorescence (XRF) spectroscopy, showing the measured silicon content compared to the calculated value, and the Ca/(P + Si) molar ratio. Carbonate content was measured from the C–H–N elemental analysis

| Sample | wt % Si (measured) | Ca/P molar ratio | Ca/(P + Si) molar ratio | wt % C (measured) |
|---|---|---|---|---|
| HA | < 0.01 | 1.67 | 1.67 | < 0.01 |
| SiHA | 0.78 | 1.74 | 1.67 | < 0.01 |

TABLE III Bulk density, packing density and specific surface area measurements of HA and SiHA granules sintered at 1200 °C for 2 h. (All densities were quoted as a percentage of the theoretical density for HA; 3.156 g $cm^{-3}$.)

| Sample | Bulk density (%) | Packing density (%) | Specific surface area (sq $mg^{-1}$) |
|---|---|---|---|
| HA | 97.2 | 43.8 | 2.36 |
| SiHA | 99.7 | 42.6 | 2.63 |

directly on the surface of the granular implants, as shown in Fig. 7. High magnification micrographs, Fig. 7(b) and (d), indicate that new bone had formed directly on the surface and within the spaces between the granules of HA and SiHA implants. There was no evidence of any inflammatory cells on the surface or between the granular implants and fibrous encapsulation was not observed. Cells such as osteoblasts and osteocytes were observed in close proximity to the implant surfaces. Active areas of bone deposition and resorption was observed occurring within all implants. Fluorescent microscopy, Fig. 8, indicates the dominant presence of layers of both alizarin red and calcein green bone marking labels in the bone tissue around the HA and SiHA granules. Both calcein green and alizarin red labels were observed continuously, in some cases in direct contact to the surface of the HA or SiHA granules and in some cases several microns away from the granule surface. In some regions (within both HA and SiHA implants), the presence of diffuse calcein green and alizarin red labels were observed, indicating woven bone, which had been rapidly formed. The intensity of the tetracycline label was very weak, possibly due to bleaching under UV light during fluorescent microscopy. The primary direction of bone ingrowth seemed to occur from the deep end toward the superficial end of the defect, with additional bone ingrowth from the walls of the defect.

### 3.4. Histomorphometry

A quantitative assessment of the area of bone ingrowth, Fig. 9, indicates that the absolute percentage of bone ingrowth for SiHA implants ($37.52\% \pm 5.87$) was significantly greater than that for HA ($21.99\% \pm 6.85$) granular implants. In addition the area of bone coverage or bone on-growth (a measurement of the amount of contact between the implant and bone), as shown in Fig. 10 was significantly greater for SiHA ($59.77\% \pm 7.34$) implants compared to HA ($47.08\% \pm 3.60\%$) implants. The bone mineral apposition rates for all implants were calculated during weeks 1–2 after implantation. Determination of the apposition rates between weeks 2 and 3 was not possible, due to the weak intensity of the tetracycline label which was administrated 3 weeks after surgery. The bone mineral apposition rates, Fig. 11, for SiHA ($3.91 \pm 0.27$ μm/day) implants were again significantly greater than that for phase pure HA ($2.53 \pm 0.29$ μm/day).

## 4. Discussion

Recent studies have highlighted how the *in vitro* bioactivity of hydroxyapatite can be enhanced with the incorporation of small levels of physiologically relevant ions such as silicate [15], carbonate [22] or magnesium [23] ions into the hydroxyapatite lattice. *In vivo* studies on these synthetic substituted hydroxyapatites are, however limited in number and quality, one of the reasons is that the physical properties of the substituted hydroxyapatite implants used, e.g. shape, size, and density may be very different from the control, normally HA implants. In addition, the synthesis methods employed to prepare substituted hydroxyapatites, often result in the presence of secondary phases or the added substitution of unwanted secondary ions, which can have a detrimental affect on the *in vivo* properties of these substituted apatites.

In this study granules (0.5–1 mm diameter) of phase pure hydroxyapatite and 0.8 wt % silicon substituted hydroxyapatite were prepared with similar physical properties. The synthesis route used to prepare a 0.8 wt % silicon substituted HA was successful and the desired amount of silicon in the sintered granules was achieved, as demonstrated by the XRF results. The XRF results also reveal that the number of phosphate groups in the SiHA granules was reduced, as indicated by the higher Ca/P molar ratio compared to HA granules. However, the Ca/(P + Si) molar ratio for SiHA was calculated as 1.67, which is equivalent to that for phase pure HA. The XRF results suggest that the silicon was

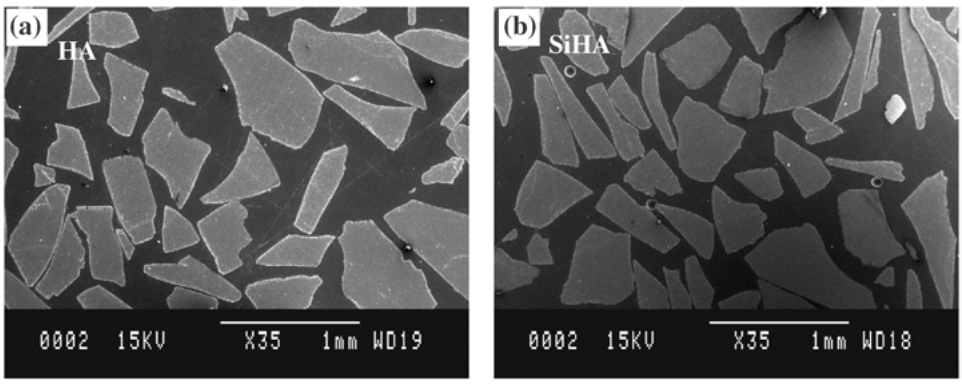


*Figure 6* Scanning electron micrographs showing that the sintered: (a) hydroxyapatite (HA) and (b) silicon substituted hydroxyapatite (SiHA) were similar in size and morphology.

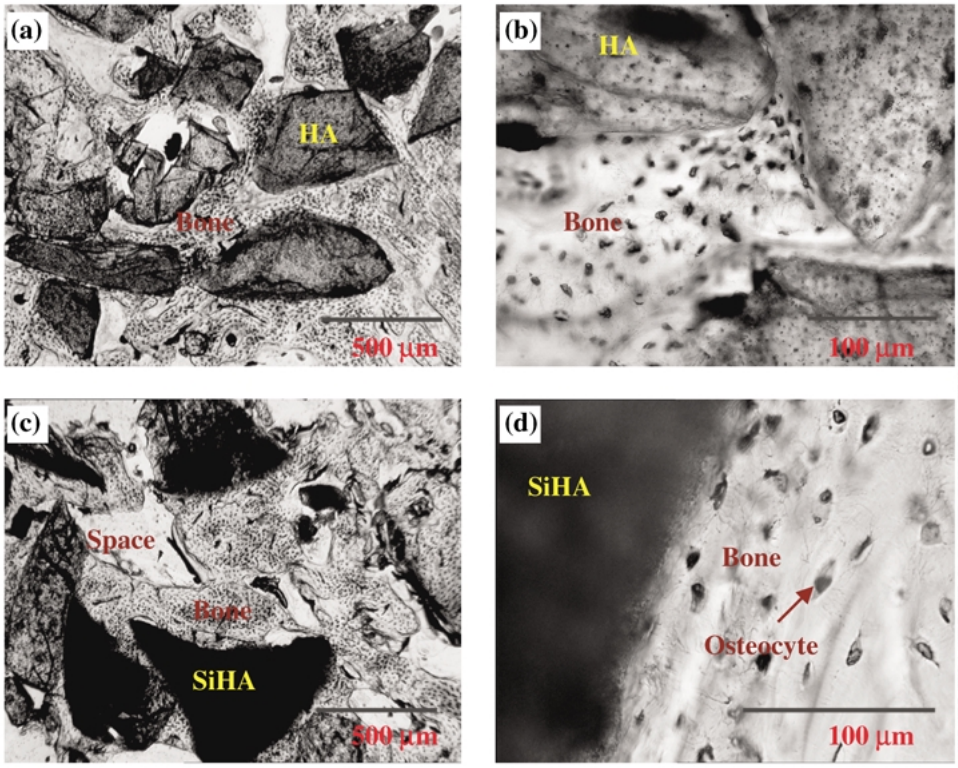


*Figure 7* Histological appearance of (a) bone ingrowth within hydroxyapatite (HA) granular implants, (b) direct bone apposition onto the surface of HA implants, (c) bone ingrowth within silicon substituted hydroxyapatite (SiHA) granular implants and (d) direct bone apposition on the surface of a SiHA granule.

incorporated into the HA lattice where it occupied the ''phosphorus site'', according to the reaction mechanism described elsewhere [14]. Further evidence of the incorporation of silicon into the HA lattice was demonstrated by the XRD data shown in Fig. 4. No secondary phases were observed for the SiHA granules, and the diffraction pattern for SiHA was identical to that of phase pure HA granules. If the silicate ions had not substituted for the phosphate site in HA, the resulting material that would have been produced would be

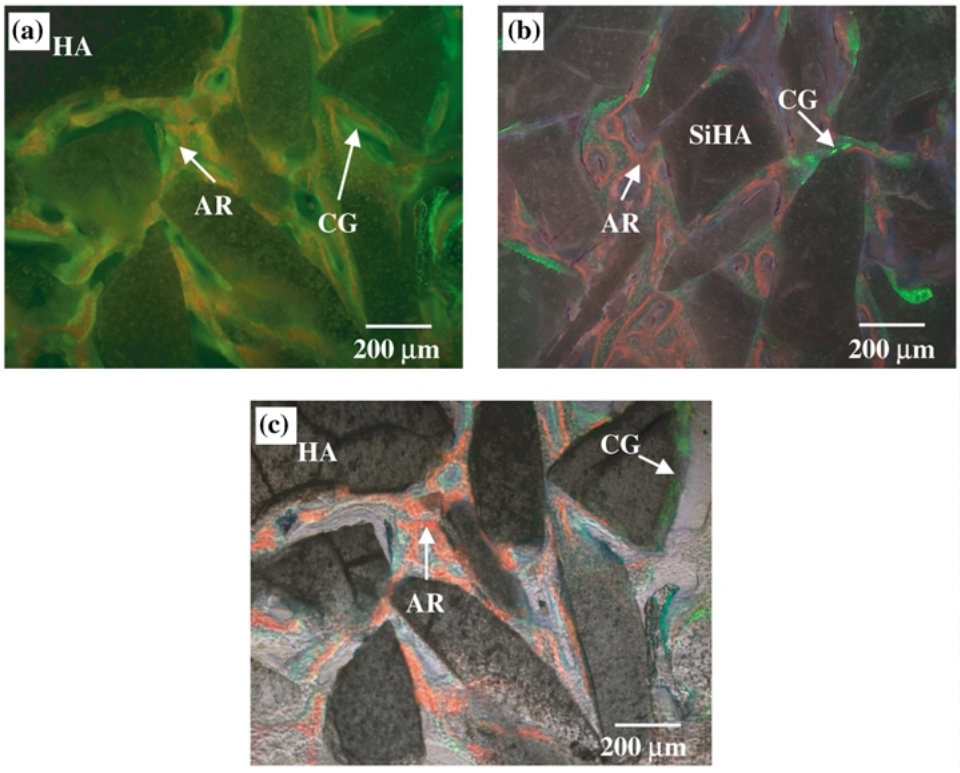


*Figure 8* Fluorochrome labeled bone within (a) hydroxyapatite (HA) implants (image acquired using a Leica N.2.1. filter cube), (b) silicon substituted hydroxyapatite (SiHA) implants (image acquired using a Leica RGB filter cube) and (c) HA implants (RGB fluorescent image superimposed onto a bright-field transmitted light image) demonstrating lamellar bone deposited at 1–2 (calcein green; CG) and 2–3 (alizarin red; AR) weeks after implantation.

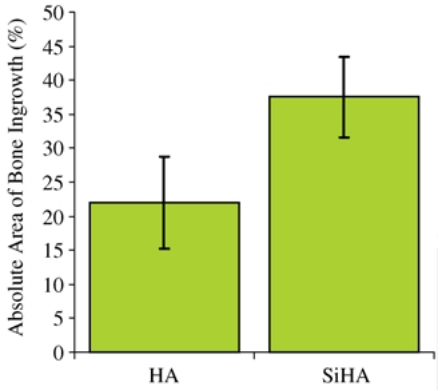


*Figure 9* Percentage of bone ingrowth within hydroxyapatite (HA) and silicon substituted hydroxyapatite (SiHA) implants ($p < 0.05$).

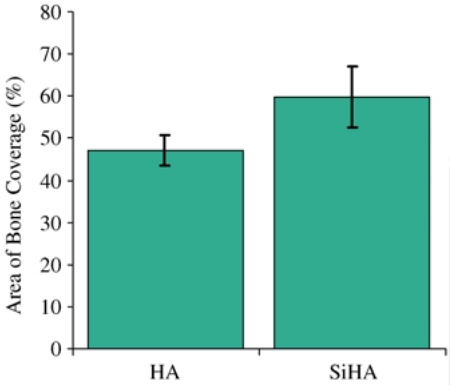


*Figure 10* Percentage of bone coverage on the surface of hydroxyapatite (HA) and silicon substituted hydroxyapatite (SiHA) implants ($p < 0.05$).

calcium rich resulting in a secondary calcium oxide phase. In this study, the XRD data revealed no secondary phases for both sintered HA and SiHA granules. FTIR spectroscopy, Fig. 5, of HA and SiHA revealed differences in the phosphate $\nu_3$ and $\nu_1$ region (1100–900 $cm^{-1}$), which was due to the substitution of silicon (or silicate) into some of the phosphorous (or phosphate) sites in HA. Furthermore no structural carbonate groups were observed by FTIR or C–H–N elemental analysis for the sintered HA and SiHA granules, demonstrating that the substitution was purely silicon (or silicate) for phosphorus (or phosphate).

Granules of HA and SiHA prepared in this study where similar in size and morphology, as indicated by the SEM images shown in Fig. 6. In addition the specific surface area, bulk density ( $\approx$ 97–98% of the theoretical) and the packing density ( $\approx$ 43%) of both HA and SiHA granules are similar (Table III) indicating that the same mass of granules were required to fill a defect of known volume. The importance of granule size, shape, bulk density and packing density of bioceramics when implanted in an osseous environment has been reported by Oonishi *et al*. [24] where they reported significant differences between osseointegration with granule size and density. Similarly Ikeda *et al*. [25] showed that the rate of bone regeneration for porous HA and apatite-wollastonite glass ceramics was dependent on granule size and porosity. In this study we prepared granules of HA and SiHA with similar size/shape, specific surface area, bulk density and packing density, prior to the application of an *in vivo* study.

The *in vivo* results indicate bone ingrowth into the spaces between both HA and SiHA granules, with direct bone contact between the granules and the surrounding bone. Both HA and SiHA implants were well accepted in the host tissue, with no evidence of inflammatory cells. No mobility between the granular implants and the bone was observed during the sectioning procedure, indicating good fixation of the implants. The absolute percentage of bone ingrowth, coverage and bone mineral apposition rate for SiHA implants was significantly greater than that for HA at 23 days *in vivo*. These findings support other *in vitro* and *in vivo* studies which have established that silicon plays an active role in bone formation and calcification [4, 5, 15]. *In vitro* studies on 0.8 and 1.6 wt % silicon substituted hydroxyaptite by Gibson *et al*. [15] have suggested that the acceleration of bone apposition for silicon substituted hydroxyapatite may partly result from an up-regulation in osteoblast cell metabolism, however the mechanism by which this occurs has to still to be resolved. Alternatively the physiological degradation properties of SiHA may differ from HA. De Bruijn *et al*. [26] reported that the *in vivo* solution-mediated degradation of a calcium phosphate was an important factor for bone/implant integration at early time points after implantation, whereby bone tissue formed more rapidly on the surface of calcium phosphates which resorbed.

Further studies are required to determine the long-term response of a range of silicon substituted hydroxyapatite implants compared to phase pure hydroxyapatite implants. This study shows clearly, however, that the biological activity/response of hydroxyapatite ceramics was significantly enhanced by the substitution of low levels of silicate ions into the HA lattice.

## 5. Conclusions

Granules of phase pure hydroxyapatite and 0.8 wt % silicon substituted hydroxyapatite with similar size, morphology, bulk density, packing density and specific surface area were prepared. The *in vivo* results from this study indicate that the bioactivity of hydroxyapatite was significantly enhanced with the addition of silicate ions into the hydroxyapatite structure. These findings suggest that silicon substituted hydroxyapatite is an improved alternative to phase pure hydroxyapatite for biomedical applications.

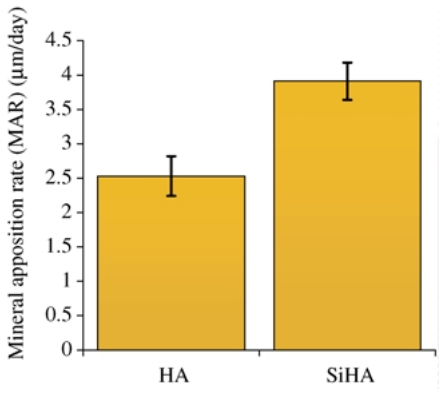


*Figure 11* Apposition rates of bone ingrowth for hydroxyapatite (HA) and silicon substituted hydroxyapatite (SiHA) implants ($p < 0.05$).

## Acknowledgments

The support of the Engineering and Physical Sciences Research Council for their funding of a studentship to N. Patel. The authors would also like to thank Mr Tom MacInnes for his assistance in processing sections for histology. Dr Roger Brooks and Dr Susan Clarke are acknowledged for their assistance in analyzing the histomorphometry data.

## References

1. N. C. BLUMENTHAL, F. BETTS and A. S. POSNER, *Calcif. Tissue Res.* **18** (1975) 81.
2. W. D. ARMSTRONG and L. SINGER, *Clinical Orthopaedics* **38** (1965) 175.
3. A. E. SOBEL, M. ROCKENMACHER and B. KRAMER, *J. Biol. Chem.* **235** (1960) 2502.
4. E. M. CARLISLE, *Science* **167** (1970) 179.
5. E. M. CARLISLE, *Calc. Tissue Int.* **33** (1981) 27.
6. K. SCHWARZ and D. B. MILNE, *Nature* **239** (1972) 333.
7. L. L. HENCH, *J. Phys.* **43** (1982) 625.
8. T. KOKUBO, S. ITO, Z. T. HUANG, T. HAYASHI, S. SAKKA, T. KITSUGI and T. YAMAMURO, *J. Biomed. Mater. Res.* **24** (1990) 331.
9. L. L. HENCH and A. E. CLARKE, in ''Biocompatibility of Orthopaedic Implants'', edited by D. F. Williams (CRC Press, Inc., 1982) Chapter 6.
10. L. L. HENCH, *J. Am. Ceram. Soc.* **74** (1991) 1487.
11. A. J. RUYS, *J. Aust. Ceram. Soc.* **29** (1993) 71.
12. K. SUGIYAMA, T. SUZUKI and T. SATOH, *J. Antibact. Antifung. Agents* **23** (1995) 67.
13. Y. TANIZAWA and T. SUZUKI, *Phosphorus Res. Bull.* **4** (1994) 83.
14. I. R. GIBSON, S. M. BEST and W. BONFIELD, *J. Biomed. Mater. Res.* **44** (1999) 422.
15. I. R. GIBSON, J. HUANG, S. M. BEST and W. BONFIELD, in ''Proceedings of the 12th International Symposium on Ceramics in Medicine, Nara, Japan, October 1999'', edited by H. Oghushi, G. W. Hastings and T. Yoshikawa (World Scientific Publishing Co., Singapure, 1999) p. 191.
16. M. AKAO, H. AOKI and K. KATO, *J. Mater. Sci.* **28** (1981) 809.
17. M. JARCHO, C. H. BOLEN, M. B. THOMAS, J. BOBICK, J. F. KAY and R. H. DOREMUS, *ibid.* **11** (1976) 2027.
18. N. PATEL, I. R. GIBSON, S. KE, S. M. BEST and W. BONFIELD, *J. Mater. Sci. Mater. in Med.* **12** (2001) 181.
19. PDF card no. 09-0432, ICDD, Newton Square, Pennsylvania, USA.
20. E. R. WEIBEL and H. E. ELIAS, in ''Quantitative methods in morphology'' (Springer-Verlag, Berlin, 1967).
21. W. A. MERZ and R. K. SCHENK, *Acta. Anat.* **76** (1970) 1.
22. K. A. HING, J. C. MERRY, I. R. GIBSON, L. DI SILVIO, S. M. BEST and W. BONFIELD, in ''Proceedings of the 12th International Symposium on Ceramics in Medicine, Nara, Japan, October 1999'', edited by H. Oghushi, G. W. Hastings and T. Yoshikawa (World Scientific Publishing Co. Singapure) p. 195.
23. T. J. WEBSTER, C. ERGUN, R. H. DOREMUS and R. BIZIOS, *J. Biomed. Mater. Res.* **59** (2002) 312.
24. H. OONISHI, L. L. HENCH, J. WILSON, F. SUGIHARA, E. TSUJI, S. KUSHITANI and H. IWAKI, *ibid.* **44** (1999) 31.
25. N. IKEDA, K. KAWANABE and T. NAKAMURA, *Biomaterials* **20** (1999) 1087.
26. J. D. DE BRUIJN, Y. P. BOVELL, J. E. DAVIES and C. A. VAN BLITTERSWIJK, *J. Biomed. Mater. Res.* **28** (1994) 105.

*Received 24 May*
*and accepted 29 May 2002*